JBC RESEARCH ARTICLE

ER entry pathway and glycosylation of GPI-anchored proteins are determined by N-terminal signal sequence and C-terminal GPI-attachment sequence

Received for publication, May 9, 2022, and in revised form, August 20, 2022 Published, Papers in Press, August 31, 2022,
https://doi.org/10.1016/j.jbc.2022.102444

Tetsuya Hirata[1], Jing Yang[2], Seita Tomida[1,3], Yuko Tokoro[1], Taroh Kinoshita[4,5,6], Morihisa Fujita[1,2], and Yasuhiko Kizuka[1,*]

From the [1]Institute for Glyco-core Research (iGCORE), Gifu University, Gifu, Japan; [2]Key Laboratory of Carbohydrate Chemistry and Biotechnology, Ministry of Education, School of Biotechnology, Jiangnan University, Wuxi, China; [3]Graduate School of Natural Science and Technology, Gifu University, Gifu, Japan; [4]Research Institute for Microbial Diseases, Osaka University, Suita, Japan; [5]WPI Immunology Frontier Research Center, Osaka University, Suita, Japan; [6]Center for Infectious Disease Education and Research, Osaka University, Suita, Japan

Edited by Phyllis Hanson

Newly synthesized proteins in the secretory pathway, including glycosylphosphatidylinositol (GPI)-anchored proteins (GPI-APs), need to be correctly targeted and imported into the endoplasmic reticulum (ER) lumen. GPI-APs are synthesized in the cytosol as preproproteins, which contain an N-terminal signal sequence (SS), mature protein part, and C-terminal GPI-attachment sequence (GPI-AS), and translocated into the ER lumen where SS and GPI-AS are removed, generating mature GPI-APs. However, how various GPI-APs are translocated into the ER lumen in mammalian cells is unclear. Here, we investigated the ER entry pathways of GPI-APs using a panel of KO cells defective in each signal recognition particle–independent ER entry pathway—namely, Sec62, GET, or SND pathway. We found GPI-AP CD59 largely depends on the SND pathway for ER entry, whereas prion protein (Prion) and LY6K depend on both Sec62 and GET pathways. Using chimeric Prion and LY6K constructs in which the N-terminal SS or C-terminal GPI-AS was replaced with that of CD59, we revealed that the hydrophobicity of the SSs and GPI-ASs contributes to the dependence on Sec62 and GET pathways, respectively. Moreover, the ER entry route of chimeric Prion constructs with the C-terminal GPI-ASs replaced with that of CD59 was changed to the SND pathway. Simultaneously, their GPI structures and which oligosaccharyltransferase isoforms modify the constructs were altered without any amino acid change in the mature protein part. Taking these findings together, this study revealed N- and C-terminal sequences of GPI-APs determine the selective ER entry route, which in turn regulates subsequent maturation processes of GPI-APs.

Most eukaryotic proteins synthesized in the cytosol need to be transported to various organelles, including mitochondria, peroxisomes, nuclei, and the endoplasmic reticulum (ER), so cells have protein transport machinery that selectively targets each organelle. Approximately one-third of proteins are destined to be transported to the ER to enter the secretory pathway and be further transported to their final destination (1, 2). The correct ER entry of newly synthesized secretory and transmembrane proteins is achieved by two major ER entry pathways: signal recognition particle (SRP)–dependent and SRP-independent pathways (3). The substrates of the SRP-dependent pathway contain a hydrophobic sequence such as a signal sequence (SS) and a transmembrane domain at or near their N termini. SRP interacts with these hydrophobic sequences during translation on the ribosomes and then recruits nascent proteins to the ER by binding to the ER-resident SRP receptor, which is an auxiliary subunit of the Sec61 translocon complex, thereby facilitating the cotranslational translocation of nascent proteins into the ER lumen (4–6). Meanwhile, some proteins containing SSs are known to be recruited to the ER in SRP-independent manners (3, 7). They are posttranslationally translocated into the ER by the other Sec61 complex, in which Sec62 and Sec63 are included as auxiliary subunits (Fig. 1*A* upper, Sec62 pathway) (8).

Another class of SRP-independent substrates is tail-anchored (TA) proteins, which have a transmembrane domain immediately adjacent to the C termini (9). The major TA proteins are soluble N-ethylmaleimide-sensitive factor attachment protein receptors (SNAREs). TA proteins are not translocated into the ER lumen, but their C termini are posttranslationally inserted into the ER membrane through the guided entry of TA proteins (GET) pathway (Fig. 1*A* upper, GET pathway) (10–12). TRC40 (GET3 in yeast) directly binds to the transmembrane domains of TA proteins (13) and then posttranslationally recruits TA proteins to the ER by interacting with the ER-resident TRC40 receptor, WRB/CAML (GET1/GET2) heterocomplex (11, 14–16). WRB/CAML complex then inserts TA proteins into the ER membrane, completing the biogenesis of TA proteins (17). Other transmembrane proteins, whose transmembrane domains are located in the middle parts of proteins, have recently been revealed to be targeted to the ER through the SND (SRP-

* For correspondence: Yasuhiko Kizuka, kizuka@gifu-u.ac.jp.

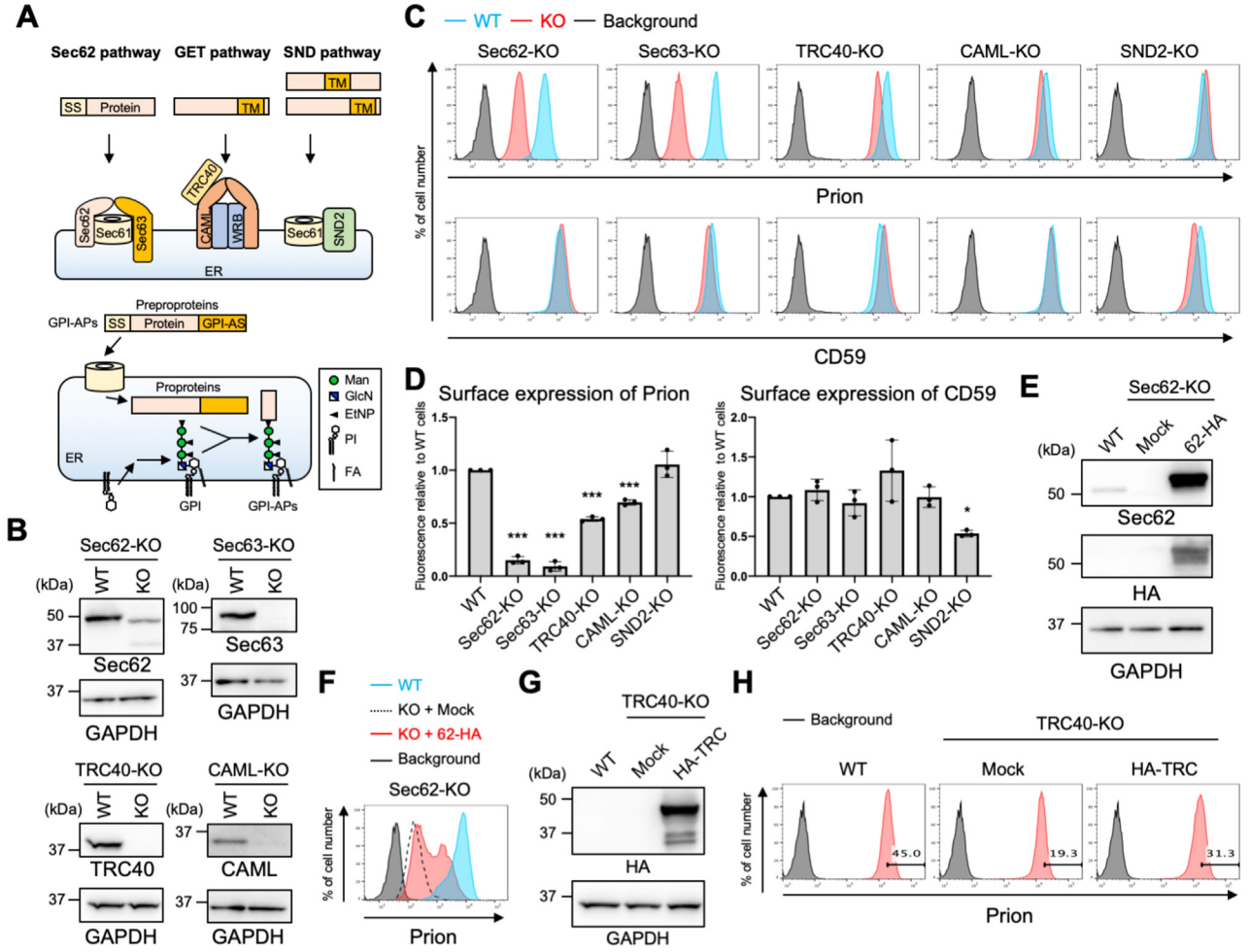

Figure 1. The distinct ER entry pathways of two GPI-APs, Prion, and CD59. *A*, (Upper) schematic of three signal recognition particle (SRP)–independent ER entry pathways. Proteins that are dependent on the Sec62 pathway have an N-terminal signal sequence (SS) (left). Tail-anchored proteins with a C-terminal transmembrane domain are dependent on the GET pathway (middle). Proteins that have a transmembrane domain in their middle or C-terminal part are dependent on the SND pathway (right). (Lower) Schematic of biosynthesis of GPI-APs. GPI is synthesized from PI in the ER. Preproproteins of GPI-APs are synthesized and translocated into the ER lumen where SSs are removed. GPI-ASs of proproteins of GPI-APs are removed and GPI is attached to newly exposed C termini, generating GPI-APs. SS, signal sequence; GPI-AS, GPI-attachment sequence; TM, transmembrane domain; Man, mannose; GlcN, glucosamine; EtNP, ethanolamine phosphate; PI, phosphatidylinositol; FA, fatty acid. *B*, lysates of HEK293 (WT), HEK293-Sec62-KO, HEK293-Sec63-KO, HEK293-TRC40-KO, and HEK293-CAML-KO cells were Western blotted for Sec62, Sec63, TRC40, CAML, and GAPDH. *C*, the surface expression of Prion and CD59 in WT and KO cells was detected by FACS. Cells were stained with anti-Prion or anti-CD59 antibodies. *D*, quantification of relative fluorescence intensity of Prion (left) and CD59 (right) in KO cells to that in WT cells is shown. Error bars represent SD ($n = 3$). Statistical analysis was performed by one-way ANOVA with *post hoc* Dunnett test. *E*, lysates of HEK293 WT and Sec62-KO cells transfected with empty vector (mock) or 3HA-tagged human Sec62 (62-HA) were Western blotted for Sec62, HA, and GAPDH. *F*, the surface expression of Prion in WT and Sec62-KO cells transfected with mock or Sec62-HA was detected by FACS. Cells were stained with anti-Prion antibodies. *G*, lysates of WT and HEK293-TRC40-KO cells transfected with empty vector (mock) or 3HA-tagged human TRC40 (HA-TRC) were Western blotted for HA and GAPDH. *H*, the surface expression of Prion in WT and TRC40-KO cells transfected with mock or HA-TRC40 was detected by FACS. Cells were stained with anti-Prion antibodies. The numbers indicate percentage of gated region in each panel. * $p < 0.05$; *** $p < 0.0005$. ER, endoplasmic reticulum.

independent) pathway (Fig. 1*A* upper, SND pathway) (18, 19). In mammalian cells, SND2 (also known as TMEM208) has been identified as the putative ER-resident receptor for SND pathway-dependent substrates (19, 20) and shown to interact with the Sec61 translocon (19, 21). SND2 is also involved in the ER entry of small secretory proteins, C-terminally transmembrane proteins, and multipass transmembrane proteins (19, 22, 23), although the precise mechanisms for SND pathway-dependent protein translocation are unknown. These SRP-independent pathways have partially overlapping functions (20), and it is unclear how an ER entry pathway is determined for each substrate. Therefore, identification of the requirements for entering each pathway is particularly important to obtain a comprehensive overview of protein entry into the ER.

In the secretory pathway, after the translocation of proteins into the ER lumen, glycosylation takes place, which is one of the most abundant posttranslational modifications of proteins and regulates protein folding, localization, and functions (24). Mammalian cell surfaces are covered with various types of glycans including *N*-glycans, *O*-glycans, glycosphingolipids, and glycosylphosphatidylinositol (GPI) (24, 25). GPI is a glycolipid modification that is attached to C termini of proteins (26, 27). Mammalian GPI is composed of a common

core structure, EtNP-6Manα1–2Manα1–6(EtNP)Manα1–4GlcNα1-6*myo*inositol-phospholipid (where EtNP, Man, and GlcN are ethanolamine phosphate, mannose, and glucosamine, respectively), and glycan side chains (26, 27). In mammalian cells, more than 150 proteins are anchored to the cell surface through GPI anchorage and localized to lipid rafts (28). GPI-anchored proteins (GPI-APs) are involved in various biological phenomena such as fertilization, early embryonic development, synaptic formation, and immunological regulation. Furthermore, abnormalities of GPI-AP expression or GPI structures cause severe disorders such as paroxysmal nocturnal hemoglobinuria and inherited GPI deficiency, the symptoms of which include hemolytic anemia, and epilepsy and developmental delay, respectively (29–31). In addition, GPI-glycan structures are involved in the pathology of prion diseases (32).

The biosynthesis of GPI-APs occurs in the ER where the biosynthesis of the protein part and GPI moiety are carried out separately (Fig. 1*A* lower) (26, 27). Precursor proteins that are destined to be modified with GPI are synthesized in the cytosol as preproproteins, which contain N-terminal SSs, mature protein parts, and C-terminal GPI-attachment SSs (GPI-ASs; Fig. 1*A* lower) (26). The preproproteins of GPI-APs are translocated into the ER lumen where SSs are removed by the signal peptidase complex (33, 34). Meanwhile, GPI is synthesized from phosphatidylinositol through sequential enzymatic reactions, and the synthesized GPI moiety is *en bloc* transferred to the nascent proproteins by GPI transamidase, which removes GPI-ASs from the proproteins and adds a GPI moiety to the newly exposed C termini of mature proteins, generating GPI-APs (Fig. 1*A* lower) (35, 36). The GPI moiety of nascent GPI-APs is then structurally remodeled by post-GPI attachment to proteins (PGAPs) in the ER and Golgi to acquire mature GPI glycolipid (37–42), and GPI-APs are finally transported to the cell surface (26, 27).

Although the biosynthetic pathway of the GPI moiety has been well characterized (26, 27), study of how the preproproteins of GPI-APs are translocated into the ER has only just been initiated. In yeast, it has been reported that large amounts of GPI-APs are translocated into the ER lumen by two SRP-independent pathways, GET and SND pathways, and these pathways are suggested to compensate each other (18, 43). Similarly, we have recently reported the contribution of the SND pathway to the expression of GPI-APs in mammalian cells. Knocking out SND2 in HEK293 cells decreased the surface expression of several GPI-APs including CD59 by approximately 50% (21). Low hydrophobicity of GPI-AS was the key for determining the dependence on the SND pathway (21). Moreover, a previous *in vitro* study suggested that prion protein (Prion), another GPI-AP, is translocated into the ER lumen in a Sec62-dependent manner (44). Consistent with this, recent genome-wide screening identified both Sec62 and Sec63 as factors required for the cell surface expression of Prion (45). These studies highlighted that SRP-independent pathways are dominant ER entry routes for GPI-APs in both yeast and mammalian cells. However, it remains elusive how each SRP-independent pathway contributes to the translocation of a wide variety of GPI-APs in mammalian cells.

Here, we investigated the translocation pathways of various GPI-APs across the ER membrane and found that CD59 is dominantly translocated into the ER by the SND pathway, while Prion and LY6K depend on both Sec62 and GET pathways. Furthermore, chimeric Prion, whose ER entry pathway was altered to that of CD59, was found to be differently modified by GPI and *N*-glycans compared with WT Prion. Our work provides insights into both how GPI-APs are translocated into the ER lumen and the importance of the ER entry pathways of GPI-APs for their GPI remodeling and *N*-glycosylation.

Results

The distinct ER entry pathways of two GPI-APs: prion and CD59

To investigate the ER entry pathways of two GPI-APs, Prion and CD59, we generated a panel of KO HEK293 cells defective in each gene for three SRP-independent pathways: Sec62 or Sec63 for the Sec62 pathway, TRC40 or CAML for the GET pathway, and SND2 for the SND pathway. The successful KO of these genes was confirmed by genotyping PCR (Fig. S1*A*) and Western blotting (Fig. 1*B*). We then examined the surface expression of endogenous Prion and CD59 in these KO cells by fluorescence-activated cell sorting (FACS). The surface expression of Prion was decreased by approximately 90% in both Sec62-KO and Sec63-KO cells compared with that in WT cells, whereas that of CD59 in Sec62-KO cells and Sec63-KO cells was comparable to that in WT cells (Fig. 1, *C* and *D*). Re-expression of 3 × HA-tagged Sec62 (62-HA) in Sec62-KO cells restored the surface expression of Prion (Fig. 1, *E* and *F*), demonstrating that the Sec62 pathway is essential for Prion but not CD59 biogenesis. Furthermore, we found that TRC40-KO cells and CAML-KO cells showed approximately 50% and 30% reductions of the surface expression of Prion, respectively (Fig. 1, *C* and *D*), and re-expression of 3 × HA-tagged TRC40 (HA-TRC) in TRC40-KO cells rescued this (Fig. 1, *G* and *H*). Similar to the case of Sec62-KO cells, however, neither TRC40-KO cells nor CAML-KO cells showed a decrease in the surface expression of CD59 (Fig. 1, *C* and *D*). These results indicate that the GET pathway is also involved in GPI-AP biogenesis in mammalian cells in a substrate-dependent manner. Western blotting of transfected Prion in CAML-KO and Sec62-KO cells showed the reduction of total expression of Prion in these KO cells and the robust increase in the Prion expression in Sec62-KO cells by the inhibition of proteasomes with MG-132 treatment, demonstrating that preproprotein of Prion is preferentially degraded by proteasomes (Fig. S2, *A* and *B*). By contrast, knocking out SND2 hardly impaired the surface expression of Prion, but instead, the surface expression of CD59 was decreased to approximately 50% in SND2-KO cells compared with that in WT cells (Fig. 1, *C* and *D*). Western blotting confirmed that cellular expression of FLAG-tagged CD59 was greatly decreased in SND2-KO cells (Fig. S2*C*). These results are consistent with a previous study (21) and

indicate that CD59 predominantly depends on the SND2 pathway among these three ER entry pathways. These results clearly indicate that two GPI-APs, Prion and CD59, utilize distinct ER targeting and translocation routes for their biogenesis. Regarding CD59, we previously showed the involvement of SRP receptor for the ER entry (21), and this was confirmed by knocking out *SRPRA* (encoding SRP receptor α) (Fig. S3).

Interaction between Sec62 pathway proteins and GET pathway proteins

Because the GET pathway functions in the ER targeting and insertion into the ER membrane of the TA protein, translocation of Prion into the ER across the membrane is unlikely to be completed by the GET pathway alone. Considering that the Sec62/Sec63 complex regulates Sec61 channel opening and provides a pulling force to thread the nascent proteins into the ER lumen (22), we hypothesized that Sec62 pathway proteins and GET pathway proteins physically interact and are functionally coupled with each other. To investigate this possibility, we performed coimmunoprecipitation experiments. FLAG-tagged Sec62 (Sec62-FLAG) was cotransfected with one of the three GET pathway proteins, CAML, HA-tagged WRB (WRB-HA), or HA-tagged TRC40 (HA-TRC40), into HEK293 WT cells, and Sec62-FLAG was immunoprecipitated with anti-FLAG beads. Not only the two ER membrane components, CAML and WRB-HA, but also a cytosolic chaperone, HA-TRC40, were coimmunoprecipitated with Sec62-FLAG (Fig. 2*A*). These results indicate the interaction between Sec62 complex and GET complex in the ER. To examine whether such physical interaction contributes to mutual stabilization of the complexes, we investigated the protein levels of each component in Sec62 pathway–defective or GET pathway–defective cells. In Sec62-KO and Sec63-KO cells, the

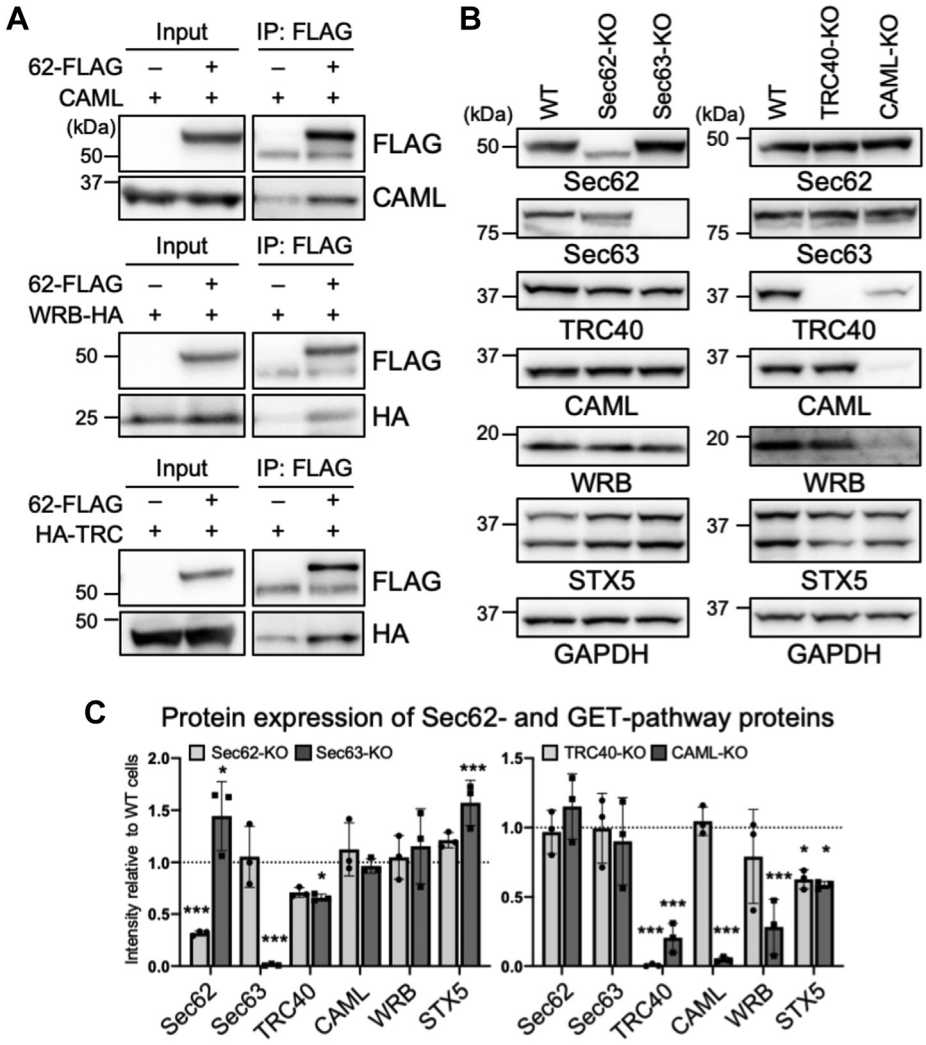

Figure 2. Interaction between Sec62 pathway proteins and GET pathway proteins. *A*, coimmunoprecipitation of CAML, WRB-3HA (WRB-HA), and 3HA-TRC40 (HA-TRC) with Sec62-3FLAG (62-FLAG). Sec62-3FLAG and CAML, WRB-3HA, and 3HA-TRC40 were coexpressed in HEK293 cells and Sec62-3FLAG was immunoprecipitated with anti-FLAG beads. Sec62-3FLAG, CAML, WRB-3HA, and 3HA-TRC40 were detected by Western blotting. *B*, lysates of HEK293 WT, Sec62-KO, Sec63-KO, TRC40-KO, and CAML-KO cells were Western blotted for Sec62, Sec63, TRC40, CAML, WRB, STX5, and GAPDH. *C*, quantification of relative band intensities of Sec62 pathway and GET pathway proteins in Sec62-KO, Sec63-KO, TRC40-KO, and CAML-KO cells to those in WT cells. Error bars represent SD ($n = 3$). Statistical analysis was performed by one-way ANOVA with *post hoc* Dunnett test. * $p < 0.05$; *** $p < 0.0005$. GET, guided entry of TA proteins.

protein levels of two GET pathway proteins (CAML and WRB) were comparable to those in WT cells (Fig. 2, *B* and *C*, left), while that of TRC40 was significantly decreased (Fig. 2, *B* and *C*, left). The partial reduction of TRC40 protein might be accounted for by the physical interaction between TRC40 and Sec62 (Fig. 2*A*). We noticed that the Sec62 protein level was increased in Sec63-KO cells, suggesting the presence of mechanisms compensating for loss of the Sec62 pathway (Fig. 2, *B* and *C*, left). In TRC40-KO and CAML-KO cells, the levels of Sec62 pathway proteins (Sec62 and Sec63) were almost the same as those in WT cells, although that of WRB protein in TRC40-KO cells and those of TRC40 and WRB in CAML-KO cells were slightly and greatly decreased, respectively (Fig. 2, *B* and *C*, right). In addition to the protein levels of Sec62 and GET pathway components, the level of one SNARE protein, syntaxin 5 (STX5), was also examined as a representative TA protein. The levels of long and short isoforms of STX5 protein were decreased in both TRC40-KO and CAML-KO cells, as expected, whereas those in Sec62-KO and Sec63-KO cells were slightly but significantly increased compared with those in WT cells (Fig. 2, *B* and *C*), confirming that the Sec62 pathway is not required for the biogenesis of TA proteins. These results indicate that physical interaction between Sec62 complex and GET complex is basically dispensable for protein stability of the counterpart complex but instead they function cooperatively for Prion biogenesis.

Hydrophobicity of N-terminal SS determines the dependence of prion on Sec62 pathway

Next, we investigated the elements in Prion required for its Sec62-dependent ER entry. To this end, we constructed chimeric Prions in which N-terminal SS and/or C-terminal GPI-AS were replaced with the CD59 sequences (Fig. 3*A*). We then analyzed the surface expression of the chimeric Prion proteins in Sec62-KO cells by FACS. To normalize transfection efficiency, the fluorescence intensity of Prion (encoded by the *PRNP* gene) was compared in the cells having the same fluorescence intensity range of ZsGreen1, which is expressed downstream of the *PRNP-IRES2* sequence (Fig. S4*A*). Whereas all Prion constructs were expressed at similar levels in WT cells (Fig. S4*B*), the surface expression of WT Prion (PPP) was drastically decreased in Sec62-KO cells compared with that in WT cells (Fig. 3, *B* and *C*), as expected from the results for

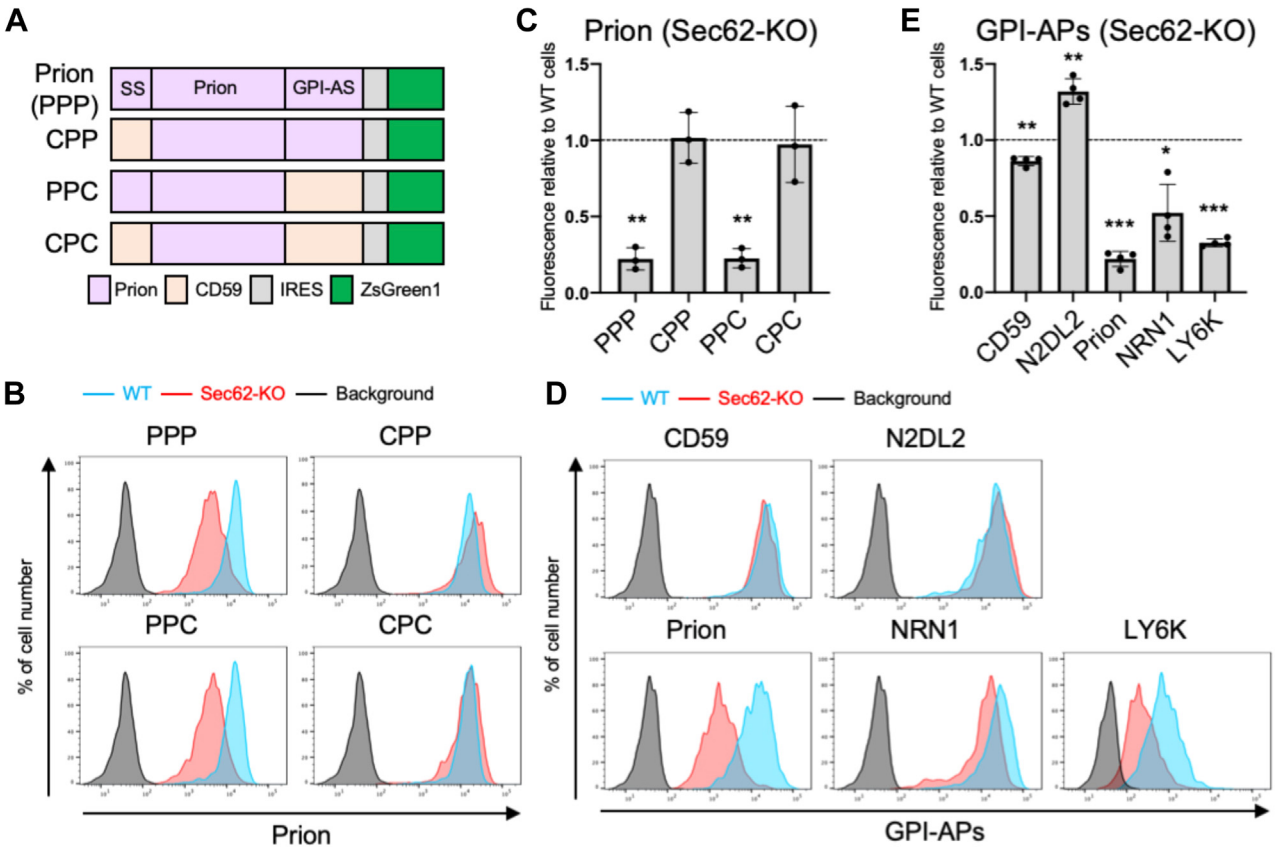

Figure 3. The hydrophobicity of N-terminal signal sequences determines the dependence on the Sec62 pathway. *A*, schematic of chimeric Prion constructs with CD59. N-terminal signal sequence (SS), C-terminal GPI-attachment sequence (GPI-AS), or both in Prion constructs were replaced with those of CD59. PPP, N- and C-terminal Prion (WT Prion); CPP, N-terminal CD59 and C-terminal Prion; PPC, N-terminal Prion and C-terminal CD59; CPC, N- and C-terminal CD59. *B*, the surface expression of chimeric Prion proteins in Sec62-KO cells was detected by FACS. HEK293 WT and Sec62-KO cells were stained with anti-Prion antibody. *C*, quantification of relative fluorescence intensity of chimeric Prion in Sec62-KO cells to that in WT cells is shown. Error bars represent SD ($n = 3$). *D*, the surface expression of exogenous GPI-APs with different hydrophobicity in their N-terminal signal sequences. Hydrophobicity of their SSs is shown in Table 1. *E*, quantification of relative fluorescence intensity of exogenous GPI-APs in Sec62-KO cells to that in WT cells is shown. Error bars represent SD ($n = 3$). Statistical analysis was performed by Welch's *t* test. * $p < 0.05$, ** $p < 0.005$, *** $p < 0.0005$. FACS, fluorescence-activated cell sorting; GPI, glycosylphosphatidylinositol; GPI-AP, GPI-anchored protein.

endogenous Prion (Fig. 1*D*). Similarly, the surface expression of the chimera with C-terminal CD59 (PPC) was also profoundly decreased in Sec62-KO cells compared with that in WT cells (Fig. 3, *B* and *C*). In sharp contrast, the surface expression of the chimeras with N-terminal CD59 (CPP) and with both N- and C-terminal CD59 (CPC) was no longer decreased in Sec62-KO cells (Fig. 3, *B* and *C*). These results clearly indicate that N-terminal SS of Prion is required for the selectivity of the Sec62 pathway. To further clarify the required feature in SS for the selectivity of the Sec62 pathway, we compared the hydrophobicity of N-terminal SSs determined by the Kyte–Doolittle score between CD59 and Prion. This is because it has been reported that the hydrophobicity of N-terminal SSs of SRP-dependent substrates is higher than that of SRP-independent but Sec62-dependent ones in yeast (46). We therefore anticipated that this is also the case with mammalian cells. Consistent with this, the hydrophobicity score of N-terminal SS of Prion was much lower than that of CD59, which are Sec62-dependent and Sec62-independent substrates, respectively (Table 1), supporting our hypothesis. To further verify this hypothesis, the surface expression of three other GPI-APs (NRN1, N2DL2, and LY6K), whose hydrophobicity scores of SSs ranged between those of Prion and CD59, was examined in Sec62-KO cells. The surface expression levels of NRN1 and LY6K were decreased to approximately 50% and 30% in Sec62-KO cells compared with those in WT cells, whereas that of N2DL2 in Sec62-KO cells was comparable to that in WT cells (Fig. 3, *D* and *E*). Notably, the hydrophobicity scores of SSs of CD59 and N2DL2 were higher than that of Prolactin, a major SRP-dependent substrate (47), whereas those of NRN1, LY6K, and Prion were lower than that of Prolactin (Table 1). These results indicate that the lowered hydrophobicity of N-terminal SS determines dependence on the Sec62 pathway.

C-terminal GPI-attachment SS is involved in the selectivity to GET pathway

We next focused on the GET pathway. It has been reported that TRC40 interacts with TA proteins through their C-terminal transmembrane domains to prevent exposure of their hydrophobic regions. Given that GPI-ASs have a hydrophobic region possibly acting as a transmembrane segment (48), we hypothesized that the hydrophobicity of C-terminal GPI-ASs is a key for GET dependence. We compared the hydrophobicity of C-terminal GPI-ASs indicated by the Kyte–Doolittle score between CD59 and Prion and found that the hydrophobicity of GPI-AS of Prion was much higher than that of CD59 (Table 2). To examine the aforementioned hypothesis, the surface expression of three other GPI-APs (N2DL2, NRN1, and LY6K), whose hydrophobicity scores of GPI-ASs were higher than that of CD59 (21), was examined in TRC40-KO cells. The surface expression of LY6K was decreased by approximately 50%, whereas that of N2DL2 and NRN1 was hardly impaired in TRC40-KO cells (Fig. 4*A*). This indicates that GET pathway dependence is not simply determined by C-terminal hydrophobicity.

To elucidate the importance of C-terminal GPI-ASs in selectivity to the GET pathway, we constructed chimeric LY6K proteins in which N-terminal SS and/or C-terminal GPI-AS were replaced with CD59 sequences (Fig. 4*B*) and examined their surface expression in TRC40-KO cells. The surface expression levels of WT LY6K (LLL) and the chimera with N-terminal CD59 (CLL) were decreased to approximately 50% in TRC40-KO cells compared with those in WT cells (Fig. 4*C*), indicating that replacement of N-terminal SS had no impact on the ER entry of LY6K. By contrast, the surface expression of the chimeras with C-terminal CD59 (LLC) and with both N- and C-terminal CD59 (CLC) was hardly changed in TRC40-KO cells compared with that in WT cells (Fig. 4*C*). These results indicate that C-terminal GPI-AS of LY6K determines the selectivity to the GET pathway. We noticed that the surface expression of LLC and CLC was greatly increased (approximately three times) in WT cells (Fig. S5). Although the detailed mechanisms behind this were unclear, replacement of GPI-AS of LY6K to that of CD59 might stabilize the LY6K preproprotein in the cytosol.

Global mapping of hydrophobicity of N- and C-terminal signal sequences of GPI-AP precursors predicts ER entry pathway of GPI-APs

Combining the aforementioned results and our previous report showing that lowered hydrophobicity of C-terminal GPI-ASs determines the dependence on the SND pathway (21), replacement of C-terminal GPI-AS of Prion with that of CD59 is expected to alter the ER entry of Prion to the SND pathway. Based on this assumption, Prion chimeras with a part of CD59 were expressed in HEK293 WT and SND2-KO cells and analyzed by Western blotting. Although the levels of all Prion chimeras were comparable in WT cells (Fig. S6*A*), the protein levels of PPC and CPC were robustly decreased in SND2-KO cells (Fig. 5*A*, approximately 30% of those in WT cells), indicating that replacement of C-terminal GPI-AS of Prion with that of CD59 altered its ER entry pathway and induced SND pathway dependence, as expected.

Table 1
Hydrophobicity scores of N-terminal signal sequence of GPI-anchored proteins

Protein	Kyte–Doolittle score of N-terminal SS
CD59	33.6
N2DL2	29.7
Prolactin[a]	25.9
NRN1	24.8
LY6K	21.5
Prion	20.9

[a] Prolactin is not GPI-anchored protein but listed as a typical SRP-dependent substrate.

Table 2
Hydrophobicity scores of C-terminal GPI-attachment sequence of GPI-anchored proteins

Protein	Kyte–Doolittle score of C-terminal GPI-AS
N2DL2	39.6
Prion	35.8
LY6K	34.5
NRN1	34.1
CD59	17.7

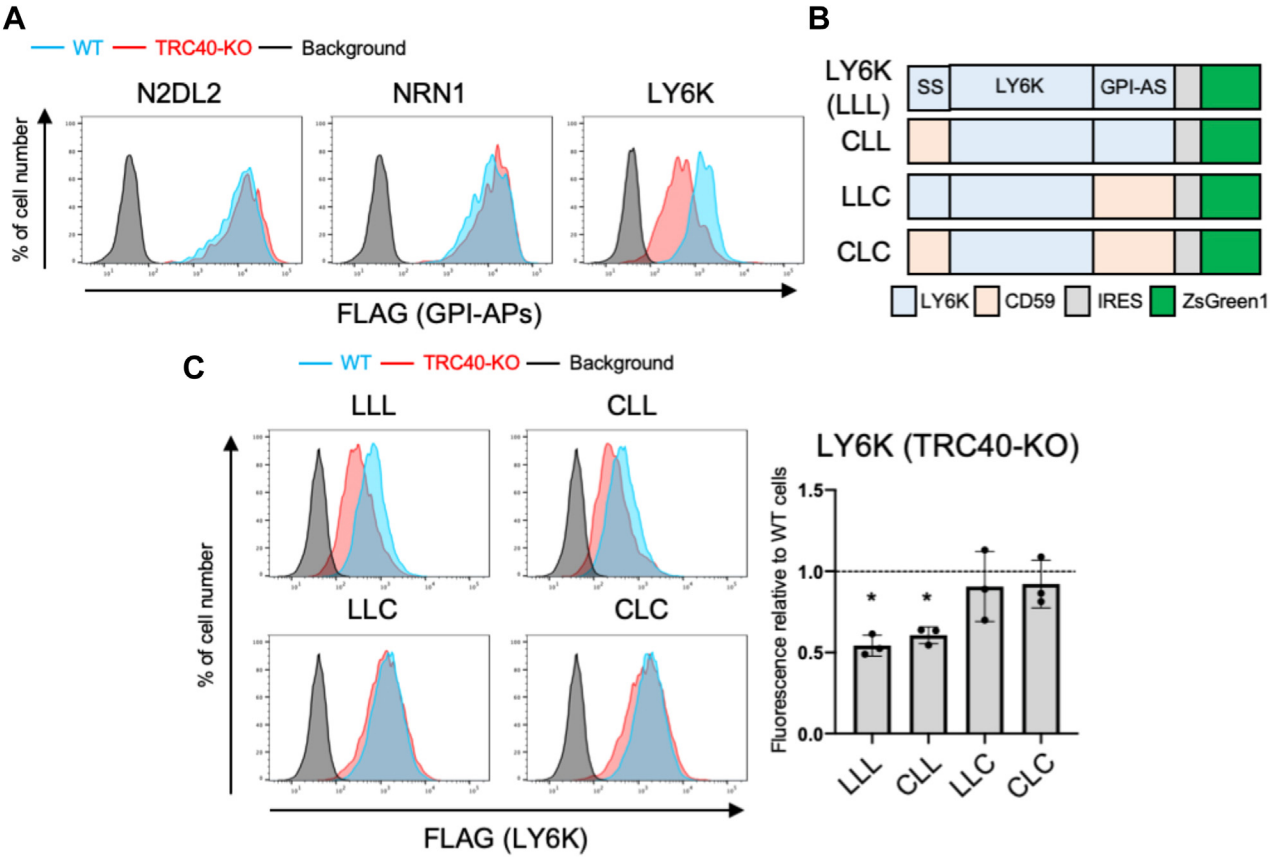

Figure 4. The C-terminal GPI-attachment sequence plays key roles for dependence on the GET pathway. *A*, the surface expression of exogenous GPI-APs with different hydrophobicity in their C-terminal GPI-ASs. Hydrophobicity of their GPI-ASs is shown in Table 2. *B*, schematic of chimeric LY6K constructs with CD59. N-terminal SS, C-terminal GPI-AS, or both in LY6K protein were replaced with those of CD59. LLL, N- and C-terminal LY6K; CLL, N-terminal CD59 and C-terminal LY6K; LLC, N-terminal LY6K and C-terminal CD59; CLC, N- and C-terminal CD59. *C*, the surface expression of the chimeric LY6K proteins in TRC40-KO cells. WT and TRC40-KO HEK293 cells were stained with anti-FLAG antibody. The graph shows the quantification of relative fluorescence intensity of chimeric LY6K in TRC40-KO cells to that in WT cells. Error bars represent SD ($n = 3$). Statistical analysis was performed by Welch's *t* test. * $p < 0.05$. GET, guided entry of TA proteins; GPI, glycosylphosphatidylinositol; GPI-AP, GPI-anchored protein; GPI-AS, GPI-attachment signal sequence; SS, signal sequence.

To visualize the relationship between the hydrophobicity of N- and C-terminal sequences and ER entry pathways, we mapped hydrophobicity scores of N-terminal SSs and C-terminal GPI-ASs of more than 130 GPI-AP preproproteins (Table S2). Proteins with N-terminal SSs with a hydrophobicity score of less than 25 (Prion, LY6K, NRN1, LLC, and PPC) utilized the Sec62-dependent pathway (Fig. 5*B*). Proteins with C-terminal GPI-ASs with a hydrophobicity score of more than 34.5 (Prion, LY6K, CPP, and CLL) utilized the GET-dependent pathway, while proteins with C-terminal GPI-ASs with lower hydrophobicity (CD59, PPC, and CPC) depended on the SND-dependent pathway (Fig. 5*B*). These results suggested that the ER entry pathway of each GPI-AP preproprotein is determined by the hydrophobicity of the N-terminal and C-terminal SSs. As mentioned previously, neither NRN1 nor N2DL2 depended on the GET pathway, suggesting the presence of other mechanisms for some GPI-AP preproproteins with higher hydrophobicity of GPI-ASs.

Alteration of ER entry pathway of prion and LY6K affects their N-glycosylation and GPI structure

Finally, we investigated the impacts of different ER entry pathways on subsequent maturation processes including glycosylation of GPI-APs. PPC and CPC in WT cells showed increased mobility in SDS-PAGE compared with WT Prion (PPP) (Fig. 5*A*), suggesting that their *N*-glycosylation states were altered. To confirm this, *N*-glycans were removed with peptide *N*-glycosidase F (PNGase F) and analyzed by Western blotting. Although PNGase F treatment generated multiple Prion bands due to the proteolytic cleavage in the post-Golgi compartment, generating smaller Prion protein fragments (49), this diminished the difference in mobility between PPP and PPC or CPC (Fig. S6*B*). This clearly indicated that *N*-glycosylation states were altered in PPC and CPC. *N*-glycosylation is carried out in the ER lumen by oligosaccharyltransferase (OST) complexes, and there are two types of OST, OSTA and OSTB, in which STT3A and STT3B are the catalytic subunits, respectively (50). As these two OST complexes *N*-glycosylate their substrates at different timings (cotranslational and posttranslational) in the ER lumen (51), we hypothesized that the altered ER entry pathway of Prion resulted in the altered dependence on OST complexes. To test this possibility, we first investigated the dependence on OST complexes of three GPI-APs, Prion, LY6K, and CD59, whose ER entry pathways differ. We expressed these GPI-APs in STT3A- and STT3B-KO cells (Fig. S6, *C* and *D*) and analyzed

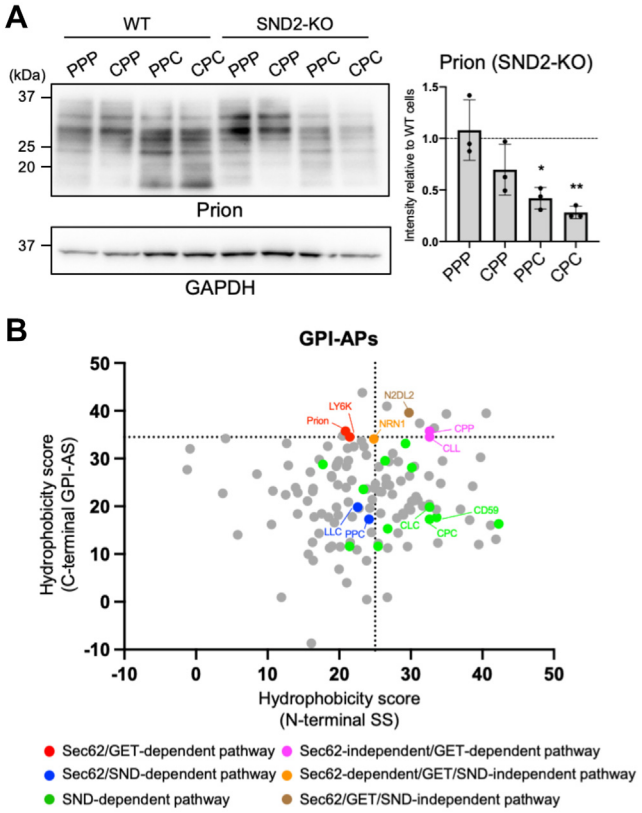

Figure 5. Global mapping of hydrophobicity of N-terminal SSs and C-terminal GPI-ASs of GPI-AP preproteins. *A*, HEK293 WT and SND2-KO cells were transfected with the plasmids for chimeric Prion proteins. Cell lysates were Western blotted for Prion and GAPDH. The graph shows the quantification of relative band intensity of chimeric Prion constructs in SND2-KO cells to that in WT cells. Statistical analysis was performed by Welch's *t* test. *B*, global mapping of hydrophobicity of N-terminal SSs and C-terminal GPI-ASs of more than 130 GPI-AP precursors. The *x*-axis indicates the hydrophobicity of N-terminal SSs and the *y*-axis indicates that of C-terminal GPI-ASs. Dotted lines indicate the borders of hydrophobicity scores for the selectivity of the ER entry (25 for the *x*-axis and 34.5 for the *y*-axis). SND-pathway dependence was based on a previous study (21) as well as this study. ER, endoplasmic reticulum; GPI, glycosylphosphatidylinositol; GPI-AP, GPI-anchored protein; GPI-AS, GPI-attachment signal sequence; SS, signal sequence.

them by Western blotting. We found that the band patterns of Prion and LY6K in STT3A-KO cells were both comparable to those in WT cells (Fig. 6*A*, left and middle, lane 1 *versus* lane 3), and the protein bands in WT and STT3A-KO cells were similarly shifted downward by removing *N*-glycans with PNGase F (Fig. 6*A*, left and middle, lane 1 *versus* lane 2, lane 3 *versus* lane 4). By contrast, the bands of Prion and LY6K migrated faster in STT3B-KO cells than in WT cells, even without PNGase F treatment (Fig. 6*A*, left and middle, lane 1 *versus* lane 5), and PNGase F treatment no longer shifted the bands (Fig. 6*A*, left and middle, lane 5 *versus* lane 6). These findings indicated that *N*-glycosylation of both Prion and LY6K is solely dependent on OSTB. Meanwhile, the band of CD59 migrated faster in both STT3A-KO and STT3B-KO cells than in WT cells (Fig. 6*A*, right, lane 1 *versus* lanes 3 and 5), and a similar migration pattern of CD59 in STT3A-KO cells was also reported previously (52), indicating that the *N*-glycosylation of CD59 depends on both OSTA and OSTB. Considering that the ER entry pathway of CD59 differs from those of Prion and LY6K, these results suggest that the dependence of OST complex is determined by the ER entry pathway of substrate proteins. To further investigate this possibility, we examined the *N*-glycosylation of the Prion and LY6K chimeras with a part of CD59 in STT3A- and STT3B-KO cells by Western blotting. The band patterns of PPP and LLL (Prion and LY6K WT) expressed in STT3A-KO cells were again comparable to those in WT cells, while they were shifted in STT3B-KO cells (Fig. 6*B*), confirming their dependence on OSTB. Intriguingly, the bands of PPC and CPC were shifted in not only STT3B-KO cells but also STT3A-KO cells (Fig. 6*B*, upper panel), indicating that these chimeras also became *N*-glycosylated by OSTA. Combined with the results of Fig. 5*A*, these results suggest that alteration of the ER entry pathway of Prion by C-terminal replacement results in the alteration of the types of OSTs involved in its *N*-glycosylation. By contrast, the migration patterns of LLC and LLL were similar (Fig. 6*B*, lower panel), suggesting that the role of C-terminal GPI-AS in *N*-glycosylation is dependent on mature protein parts. We noticed that the band patterns of CPP and CLL were less affected in both STT3A-KO and STT3B-KO cells than PPP and LLL (Fig. 6*B*), implying that these chimeras are dependent on both STT3A and STT3B. This indicates that alteration of the ER entry pathway by replacement of N-terminal SS also affects *N*-glycosylation status.

Because the altered ER entry route led to the differential OST usage, we wondered whether other posttranslational modifications carried out in the ER were also affected by ER entry pathways. GPI undergoes lipid remodeling (GPI-inositol deacylation) in the ER by PGAP1 (37), and we compared the efficiency of GPI-inositol deacylation by PGAP1 in Prion, CD59, and their chimeras. Phosphatidylinositol-specific phospholipase C (PI-PLC) cleaves GPI processed by PGAP1 but not inositol-acylated GPI (37, 53, 54). Therefore, the efficiency of GPI-inositol deacylation can be estimated from the efficiency of PI-PLC cleavage. HEK293 WT cells were treated with or without PI-PLC, and the surface expression of CD59 and Prion was analyzed by FACS. Whereas the surface expression of CD59 was drastically decreased by PI-PLC treatment (only approximately 1% of CD59 remained), that of Prion was only partially decreased (approximately 50% of Prion remained) (Fig. 6*C*). These results indicate that the efficiency of GPI-inositol deacylation by PGAP1 varies between CD59 and Prion. To examine whether an altered ER entry pathway led to the altered efficiency of GPI-inositol deacylation, we expressed the Prion chimeras in HEK293 WT cells and administered treatment with or without PI-PLC, followed by FACS analysis. Whereas the PI-PLC resistance of CPP was comparable to that of PPP, that of PPC and CPC was slightly but significantly decreased compared with that of PPP (Fig. 6*D*). These results indicate that replacement of C-terminal GPI-AS alters the efficiency of GPI-inositol deacylation by PGAP1.

Discussion

In this study, we revealed that the ER translocation of GPI-APs such as Prion and LY6K is dependent on the Sec62 and

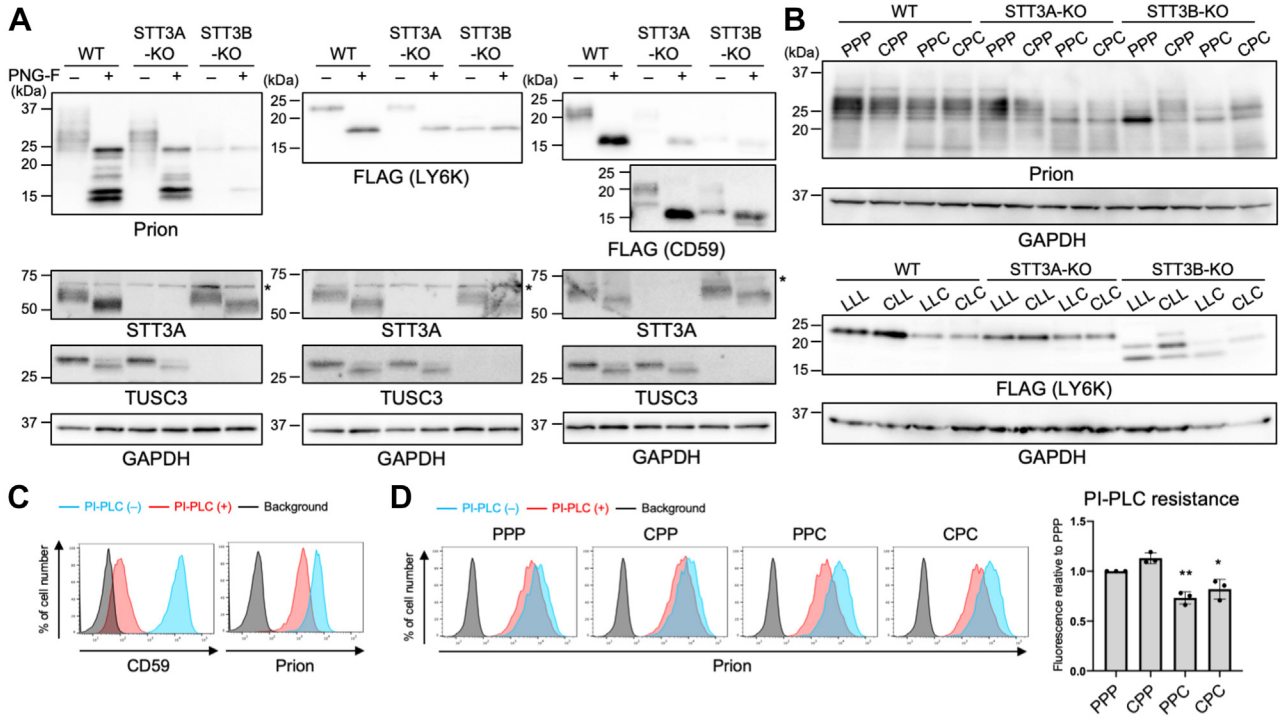

Figure 6. Alteration of the ER entry pathway of Prion and LY6K affects their *N*-glycosylation and GPI structure. *A*, HEK293 WT, STT3A-KO (clone #4), and STT3B-KO (clone #1) cells were transfected with FLAG-tagged Prion, LY6K, and CD59. Cell lysates treated with or without PNGase F (PNG-F) were Western blotted for Prion, FLAG, STT3A, TUSC3, and GAPDH. Lower panel of FLAG (CD59) shows the long-exposed image. * indicates nonspecific bands. *B*, HEK293 WT, STT3A-KO, and STT3B-KO cells were transfected with chimeric Prion and LY6K constructs. Cell lysates were Western blotted for Prion, FLAG, and GAPDH. *C*, the surface expression of CD59 and Prion treated with or without PI-PLC is shown. Cells were stained with anti-CD59 or anti-Prion antibodies. *D*, the surface expression of chimeric Prion in WT cells treated with or without PI-PLC is shown. Cells were stained with anti-Prion antibody. The graph shows the quantification of relative fluorescence intensity of chimeric Prion constructs treated with or without PI-PLC in WT cells. Error bars represent SD ($n = 3$). Statistical analysis was performed by one-way ANOVA with *post hoc* Dunnett test. * $p < 0.05$, ** $p < 0.005$. ER, endoplasmic reticulum; GPI, glycosylphosphatidylinositol.

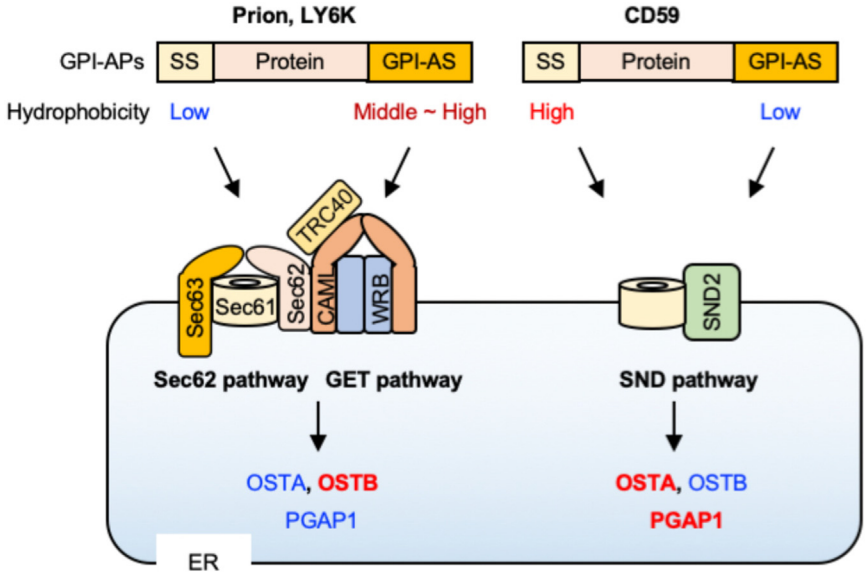

Figure 7. Possible ER import pathways and the associated glycosylation machinery for GPI-APs. The ER translocation pathways of GPI-APs are possibly determined by the hydrophobicity of their N-terminal SS and C-terminal GPI-AS. GPI-APs like Prion and LY6K, in which hydrophobicity of N-terminal SSs and C-terminal GPI-ASs is low and high, respectively, are targeted to the ER by the GET pathway, followed by import into the ER lumen in a Sec62-dependent manner. OSTB is suggested as dominant *N*-glycosylation machinery in this pathway, and GPI remodeling by PGAP1 less frequently occurs. By contrast, GPI-APs like CD59, in which hydrophobicity of N-terminal SSs and C-terminal GPI-ASs is high and low, respectively, are targeted and imported into the ER in a SND2-dependent manner. *N*-glycosylation in this pathway is likely to be mainly carried out by OSTA, and GPI remodeling by PGAP1 is efficient. Glycosylation enzymes that mainly function downstream of the pathways are indicated by bold *red* characters and those that less efficiently function are indicated by *blue* characters. ER, endoplasmic reticulum; GET, guided entry of TA proteins; GPI, glycosylphosphatidylinositol; GPI-AP, GPI-anchored protein; GPI-AS, GPI-attachment signal sequence; SS, signal sequence.

GET pathways, and the hydrophobicity of N-terminal SS and C-terminal GPI-AS is involved in the selectivity of the ER translocation pathways. In addition, the replacement of C-terminal GPI-AS of Prion altered not only its ER import pathway but also its *N*-glycosylation status and GPI structure. To summarize the results of this study and our previous report (21), the ER entry pathway of preproproteins of GPI-APs are determined by hydrophobicity of N-terminal SSs and C-terminal GPI-ASs, and subsequent maturation processes including *N*-glycosylation and GPI-remodeling are dependent on the ER entry pathway (Fig. 7). Consistent with this, a recent study has reported that Sec62 pathway–dependent substrates commonly have N-terminal SS with low hydrophobicity (55). Considering that Get3p in yeast directly binds to the C-terminal GPI attachment sequence of Gas1p (43) and that Sec62-dependent proteins could be posttranslationally translocated into the ER, we speculate that GPI-APs are posttranslationally targeted to the ER and that N-terminal signal sequences of GPI-APs do not contribute to initiating the ER targeting or do not to arrest the ribosomal translation and that C-terminal GPI-AS is a key for the ER entry.

Given that Sec61β, which is a component of the Sec61 translocon (6), is a TA protein, loss of GET pathway proteins might indirectly affect the ER translocation of Prion and LY6K by impairing the function of the Sec61 translocon. However, the direct involvement of the GET pathway in the translocation of GPI-APs is more likely for the following reasons. Firstly, the surface expression of CD59 was not changed in KO cells defective in the GET pathway, indicating that general functions of the Sec61 translocon were retained. Secondly, there were no differences in the protein levels of Sec62 and Sec63 in TRC40- and CAML-KO cells, ruling out that the Sec62 pathway was impaired in GET pathway–defective cells. Thirdly, replacement of the C-terminal GPI-AS of LY6K with that of CD59 overcame the effect of the loss of TRC40. Fourthly, a previous study revealed the direct interaction of Get3p (a TRC40 ortholog in yeast) with GPI-AS of a GPI-AP, Gas1p, in yeast (43). Finally, a previous study reported that the level of Sec61β was unaffected in GET pathway–deficient cells, probably due to the alternative membrane insertion through other ER entry pathways that have redundant function to the GET pathway (20).

It is still unclear how the ER translocation of GPI-APs is completed because GET and SND pathway proteins themselves have no activity to translocate their client proteins across the ER membrane. We here showed that Sec62 interacts with GET pathway proteins (Fig. 2). Sec62/Sec63 complex is an auxiliary subunit of the Sec61 translocon and facilitates Sec61 channel opening (22). Furthermore, Sec63 recruits an ER chaperone, BiP, through its J-domain, providing the force for threading the nascent proteins into the ER lumen (56–58). Therefore, the complex formation between Sec62 and GET pathway proteins may account for the efficient ER translocation of some GPI-APs, where GET pathway proteins recruit the GPI-APs to the ER and Sec62 pathway proteins complete their ER import. Contrary to GPI-APs, TA proteins such as SNAREs are largely dependent on the GET pathway for their targeting to the ER and do not require the Sec62 pathway (Fig. 2) (3). Therefore, only a part of GET pathway proteins likely interacts with the Sec62 complex and the GET pathway complex alone can function for TA protein biogenesis. This notion is supported by the fact that knocking out one pathway did not affect the protein levels of the other, and the level of STX5 protein was increased in Sec62-KO and Sec63-KO cells, in which the GET pathway complex would exist alone (Fig. 2). As for the SND pathway, SRP receptor is supposed to function as an auxiliary subunit of the Sec61 translocon, as we previously reported that the surface expression of CD59 was impaired by knocking down SRP receptor in WT cells but not in SND2-KO cells (21). Further *in vitro* studies testing the involvement of the Sec62 complex, GET pathway complex, SND pathway proteins, and SRP receptor in the translocation of various GPI-APs across the ER membrane are essential to fully understand the ER translocation mechanisms of GPI-APs.

Although it is reasonable that GPI-APs such as Prion and LY6K, whose C-terminal GPI-ASs are highly hydrophobic, are targeted to the ER by the GET pathway, our results indicate that dependence on the GET pathway does not simply rely on C-terminal hydrophobicity. Given that the surface expression of GPI-APs such as NRN1 and N2DL2 was unchanged in TRC40-KO cells despite the high hydrophobicity of their GPI-ASs (Fig. 4*A*), it is possible that other characteristics of GPI-ASs are also involved in determining the ER entry pathway. One possible factor might be the length of GPI-AS, as is the case for the length of C-terminal transmembrane domain of multipass transmembrane proteins (59). Alternatively, other ER entry pathways might compensate for the defects caused by loss of TRC40 for the translocation of these GPI-APs. Indeed, for the biogenesis of transmembrane proteins and TA proteins, knocking out one pathway can be compensated by alternative pathways as backup systems (20, 60). Simultaneous depletion of multiple ER entry pathways would be required to elucidate this point.

We showed that distinct ER entry pathways contribute to the differential usage of OST complexes and efficiency of the PGAP1 reaction (Fig. 6). The Sec61 translocon associates with various accessory proteins to facilitate multiple cotranslational processes, including *N*-glycosylation by OST (6). Since there are at least two types of Sec61 translocon in mammalian cells, comprising either α1 or α2 Sec61α channel (3, 61), it is possible that the types of Sec61 translocon and their interacting OST complex differ among the ER entry pathways. In this situation, the difference of Sec61α subunit might contribute to the interaction with different OSTs, leading to differential *N*-glycosylation of the same Prion protein with only different GPI-ASs. Detailed biochemical experiments are essential to clarify this point.

In addition to our present results, the involvement of C-terminal GPI-ASs in post-ER events of GPI-APs such as polarized protein transport and glycosylation was also reported. Regarding polarized protein transport, GFP bearing C-terminal GPI-AS derived from Prion was localized to the basolateral side of polarized Madin-Darby canine kidney

(MDCK) cells, whereas that bearing GPI-AS from folate receptor was on the apical side (62). Similarly, a chimeric Prion whose GPI-AS was replaced with that of Thy1 (Prion-Thy1) was reported to be relocalized from the basolateral side to the apical side in MDCK cells (63). As for glycosylation, Prion-Thy1 has been shown to be less modified with sialic acid in the Golgi on its GPI-GalNAc side chain than WT Prion (64). Another report described that *N*-glycan structures of GPI-anchored horseradish peroxidase (HRP) differ between HRP fused with GPI-AS from Thy1 and that from DAF, in which HRP-Thy1 was highly sialylated, whereas HRP-DAF had immature oligo-mannose-type *N*-glycans (65). It remains unclear how GPI-ASs are involved in polarized protein sorting and glycosylation, including GPI-GalNAcylation and sialylation of *N*-glycans, because these are carried out in the Golgi where GPI-ASs have already been removed from GPI-APs in the ER (41, 66). Therefore, GPI-ASs must affect post-ER processes of GPI-APs before their removal, probably during the translocation. Our current results provide potential initial mechanisms for aforementioned phenomena. Since we have recently reported that the loss of the GPI-GalNAc side chain accelerates the pathology of prion diseases (32), elucidation of the mechanisms by which the ER translocation pathways regulate the biological events in the Golgi will greatly advance our understanding of protein biogenesis in the secretory pathway and the mechanisms of development of prion diseases.

In summary, we revealed the roles of N- and C-terminal signal sequences for the selective ER entry and subsequent glycosylation of GPI-APs. Because GPI-APs uniquely have two hydrophobic sequences in their N and C termini, it is reasonable that they have characteristic translocation mechanisms into the ER, which will be attractive targets to fully understand the ER translocation mechanisms of proteins.

Experimental procedures

Antibodies and reagents

The following antibodies were purchased and used: rabbit anti-SEC62 and mouse anti-FLAG (clone M2) (catalog no.: HPA014059 and F1804) from Sigma–Aldrich; rabbit anti-SEC63, rabbit anti-ASNA1 (TRC40), and rabbit anti-TUSC3 (catalog no.: 13978-1-AP, 15450-1-AP, and 16039-1-AP) from ProteinTech; guinea pig anti-CAML, rabbit anti-WRB, and rabbit anti-Syntaxin 5 (catalog no.: 359004, 324103, and 110053) from Synaptic Systems; anti-β-catenin mAb (clone 14) from BD Biosciences (610154); rabbit anti-HA (clone C29F4) (catalog no.: 3724) from Cell Signaling Technology; mouse anti-GAPDH (clone 6C5) (catalog no.: MAB374) from Millipore; mouse anti-Prion (clone 4D5) (catalog no.: 14-9230-82) from eBioscience; rabbit anti-Prion (clone EP1802Y) (catalog no.: ab52604) from Abcam; mouse anti-human CD59 (clone 5H8), mouse anti-ITM1 (STT3A) (clone A-2) (catalog no.: sc-390227) from Santa Cruz; HRP-conjugated anti-mouse IgG and HRP-conjugated anti-rabbit IgG from GE Healthcare (NA931V and NA934V); HRP-conjugated anti–guinea pig IgG from ProteinTech (SA00001-12); and PE-conjugated goat anti-mouse IgG (catalog no.: 405307) from BioLegend.

The following reagents and kits were purchased and used: MG-132 (Millipore, 474790); N-glycosidase F (PNGase F) and complete mini protease inhibitor cocktail (EDTA-free) (Roche, 11365169001 and 11836170001); Pierce BCA Protein Assay Kit and Lipofectamine 3000 (Thermo Fisher Scientific, 23227 and L3000); anti-DYKDDDDK tag antibody Magnetic Beads (FLAG beads) (Wako, 017-25151); and NEBuilder HiFi DNA Assembly Master Mix (New England Biolabs, E2621).

Plasmid construction

Primers used in this study are listed in Table S1. To construct a plasmid encoding C-terminally 3 × HA-tagged Sec62, human Sec62 (hSec62) sequence was amplified from a human brain complementary DNA (cDNA) library as a template using primers (#1 and #2), followed by digestion with *Eco*RI and *Mlu*I. The sequence was ligated into pME-3HA vector digested with the same enzyme pair. pME-hSec62-3FLAG was constructed by ligation of the hSec62 sequence, which was amplified from pME-hSec62-3HA as a template using primers (#1 and #2) and digested with *Eco*RI and *Mlu*I, into the pME-3FLAG vector digested with the same enzyme pair. To construct plasmids encoding C-terminally 3 × HA-tagged WRB and N-terminally 3 × HA-tagged TRC40, cDNA sequences of hWRB and hTRC40 were amplified from a cDNA library of HEK293 cells as a template using primers (#3 and #4 and #5 and #6), followed by digestion with *Eco*RI and *Mlu*I or *Sal*I and *Not*I. The sequences were ligated into pME-3HA vector digested with the same enzyme pair. The cDNA sequence of hCAML was amplified from a human brain cDNA library as a template using primers (#7 and #8), followed by digestion with *Sal*I and *Not*I. The sequence was ligated into pME-3FLAG vector digested with the same enzyme pair. pME-hCAML (untagged) was constructed by ligation of the hCAML sequence, which was amplified from pME-3FLAG-hCAML as a template using primers (#9 and #8) and digested with *Xho*I and *Not*I, into the pME-Zeo vector digested with the same enzyme pair. cDNA sequences of mature protein parts and C-terminal GPI-ASs of hNRN1 and hLY6K were amplified from pLIB2-ssCD59-hNRN1 and pLIB2-ssCD59-hLY6K (21) as templates using primers (#10 and #11 and #12 and #13), and the same cDNA part of hN2DL2 was amplified from a human brain cDNA library as a template using primers (#14 and #15). N-terminal SSs of hNRN1 and hN2DL2 were amplified from a human brain cDNA library as a template using primers (#16 and #17 and #18 and #19) and N-terminal SS of hLY6K was obtained by the annealing of primers (#20 and #21). N-terminal SSs and mature protein sequences were ligated into pIRES2-ZsGreen1 digested with *Xho*I and *Eco*RI using NEBuilder HiFi DNA Assembly Master Mix.

To construct pME-ssPrion-FLAG-hCD59, which is a chimeric CD59 construct whose N-terminal SS was replaced with that of hPrion, pME-FLAG-hCD59 was digested with *Eco*RI and *Pst*I and ligated with the annealed primers (#22 and

#23). To generate chimeric CD59 constructs whose C-terminal GPI-ASs were replaced with that of Prion, pME-FLAG-hCD59 and pME-ssPrion-FLAG-hCD59 were digested with *Xho*I and *Not*I and ligated with the annealed primers (#24 and #25). The chimeric CD59 sequences were amplified from pME-FLAG-hCD59, pME-ssPrion-hCD59, pME-FLAG-hCD59-Prion, and pME-ssPrion-FLAG-hCD59-Prion as templates using primers (#26 and #27, #28 and #27, #26 and #29, and #28 and #29), followed by digestion with *Nhe*I and *Bam*HI. The amplified sequences were ligated into pIRES2-ZsGreen1 plasmid (Takara) digested with the same enzyme pair. The cDNA sequences of the mature protein part and C-terminal GPI-AS of hPrion were amplified from pME-ssHA-hPrion (67) as a template using primers (#30 and #29 and #31 and #29), followed by digestion with *Pst*I and *BamH*I. The amplified sequences were ligated into pIRES2-ssPrion-hCD59-Prion and pIRES2-ssCD59-hCD59-Prion digested with the same enzyme pairs. The cDNA sequences of the mature protein part of hPrion were amplified from pME-ssHA-hPrion as a template using primers (#30 and #32 and #31 and #32) and the GPI-AS of hCD59 was amplified from pME-FLAG-hCD59 as a template using primers (#33 and #34). The amplified sequences of the mature protein part of hPrion and GPI-AS of hCD59 were ligated into pIRES2-ssPrion-hCD59-Prion and pIRES2-ssCD59-hCD59-Prion digested with *Pst*I and *BamH*I using NEBuilder HiFi DNA Assembly Master Mix. To construct chimeric LY6K plasmids, the cDNA sequences of the mature protein part of LY6K were amplified from pIRES2-FLAG-hLY6K as a template using primers (#35 and #36, #37 and #38, and #35 and #38) and the GPI-AS of hLY6K was amplified from pIRES2-FLAG-hLY6K using primers (#39 and #34). The amplified sequences of the mature protein part of LY6K and the GPI-AS of hLY6K were ligated into pIRES2-ssCD59-hPrion and pIRES2-FLAG-hLY6K digested with *Pst*I and *BamH*I using NEBuilder HiFi DNA Assembly Master Mix.

To construct plasmids for gene editing, pX330-EGFP (68) and pX330-Puro (69) were digested with *Bbs*I followed by ligation with the annealed primer sets: single guide RNA (sgRNA) for human (h) *SEC62*-1, #40–#41; *hSEC62*-2, #42–#43, *hSEC63*-1, #44–#45; *hTRC40*-1, #46–#47; *hTRC40*-2, #48–#49; *hCAML*-1, #50–#51; *hCAML*-2, #52–#53; *hSND2*-1, #54–#55; *hSND2*-2, #56–#57; hSRPRA-1, #58-#59; hSRPRA-2, #60-#61; *hSTT3A*-1, #62–#63; *hSTT3A*-2, #64–#65; *hSTT3B*-1, #66–#67; and *hSTT3B*-2, #68–#69. Primers for sgRNA of *hSTT3A* and *hSTT3B* as described in previous literature were used (70).

Cell culture

HEK293 cells were obtained from ATCC. HEK293, HEK293-Sec62-KO, HEK293-Sec63-KO, HEK293-TRC40-KO, HEK293-CAML-KO, HEK293-SND2-KO, HEK293-STT3A-KO, and HEK293-STT3B-KO cell lines were cultured in Dulbecco's modified Eagle's medium supplemented with 10% fetal bovine serum at 37 °C under 5% v/v CO_2 conditions.

To inhibit protein degradation pathways, HEK293 cells were treated with 10 μM MG-132 for 24 h.

Establishment of KO cells and stable transfectants

To generate Sec62-KO, Sec63-KO, TRC40-KO, CAML-KO, and SND2-KO cell lines, one or two different pX330-EGFP plasmids harboring sgRNAs targeting each gene were transfected into HEK293 cells with Lipofectamine 3000 reagent, as described later. Two days after transfection, cells with high expression of EGFP were collected by cell sorting using FACS Melody (BD Biosciences). For STT3A-KO and STT3B-KO cell lines, pX330-Puro plasmids harboring sgRNAs targeting each gene were transfected into HEK293 cells with Lipofectamine 3000 reagent, as described later. The following day, cells were selected with 3 μg/ml puromycin for 2 days. All of the KO cell lines were established by cloning by limiting dilution. As we could not obtain any SRPRA-KO cell line, we generated bulk population of SRPRA-KO cells. We transfected pX330-Puro plasmids with sgRNAs targeting *SRPRA* gene into HEK293 cells with Lipofectamine 3000 reagent, followed by 7 days incubation with 3 μg/ml puromycin. Obtained bulk population was subjected to FACS analysis. The KO of each gene was confirmed by PCR using the following primers listed in Table S1 and Western blotting with specific antibodies: *SEC62*, #70–#71; *TRC40*, #72–#73; *CAML*, #74–#75; *SND2*, #76–#77; STT3A, #78–#79; and STT3B, #80–#81. Primers for *STT3A* and *STT3B* were used as previously described (70).

Plasmid transfection

Cells at approximately 50% confluence grown on 6 cm or 10 cm dishes were transfected with each plasmid using Lipofectamine 3000 reagent, in accordance with the manufacturer's protocol.

Sample preparation

Cells were washed with PBS twice and collected using cell scrapers, followed by precipitation by centrifugation at 1400×*g* for 3 min. The cell pellets were lysed with lysis buffer (20 mM Tris (pH 7.4), 150 mM NaCl, and 1% Triton X-100) containing protease inhibitor cocktail on ice for 30 min, followed by centrifugation at 20,000×*g* for 15 min at 4 °C. For the detection of Prion, cell lysates were prepared with lysis buffer (50 mM Tris (pH 7.4), 150 mM NaCl, 1 mM EDTA, and 60 mM Octyl-β-D-glucoside). The supernatant was recovered and the protein concentration was measured using BCA kit.

For PNGase F treatment, samples were denatured in denaturing buffer (20 mM Tris (pH 7.4), 0.5% SDS, 1% 2-mercaptoethanol, and 5 mM EDTA) at 95 °C for 5 min, followed by five times dilution with Tris-buffered saline (TBS) containing Nonidet P-40 (final concentration, 0.5%). Sixty microliters of the samples were then incubated with 3 μl of water or PNGase F at 37 °C for more than 2 h. The samples were then mixed with 5 × Laemmli SDS sample buffer and incubated at 95 °C for 5 min.

Coimmunoprecipitation

Cells grown on 10 cm dishes were transiently cotransfected with Sec62-3FLAG and CAML, WRB-3HA, or 3HA-TRC40 and cultured for 48 h. Cells were washed with PBS twice and

collected using cell scrapers, followed by precipitation by centrifugation at 1400×*g* for 3 min. Cell pellets were lysed with lysis buffer (20 mM Tris (pH 7.4), 150 mM NaCl, 1% Triton X-100) containing protease inhibitor cocktail and sonicated. The lysates were centrifuged at 20,000×*g* for 15 min at 4 °C. The supernatants were incubated with anti-FLAG beads overnight at 4 °C. The following day, anti-FLAG beads were washed with lysis buffer three times, and the beads were incubated with 50 μl of Laemmli SDS sample buffer at 95 °C for 5 min.

Western blotting

The same amounts of proteins were loaded in each well and separated by 5% to 20% SDS-PAGE, followed by transfer to nitrocellulose membranes. For Western blotting, the membranes were blocked with 5% skim milk in TBS containing 0.1% Tween-20 (TBS-T) for 30 min, followed by incubation with primary antibodies diluted with 5% skim milk/TBS-T overnight at 4 °C. After washing with TBS-T three times, the membranes were then incubated with secondary antibodies conjugated with HRP for 1 h at room temperature. Signals were detected using FUSION SOLO 7s EDGE (Vilber). Dilution rates of antibodies and lectins were as follows: anti-Sec62 (1:500), anti-Sec63 (1:500), anti-TRC40 (1:500), anti-CAML (1:500), anti-WRB (1:250), anti-STX5 (1:1000), anti-GAPDH (1:2000), anti-FLAG (1:1000), anti-HA (1:2000), rabbit anti-Prion (1:500), anti-STT3A (1:500), anti-TUSC3 (1:300), anti-mouse IgG-HRP (1:10,000), anti-rabbit IgG-HRP (1:20,000), and anti–guinea pig IgG-HRP (1:10,000).

FACS analysis

Cells were washed with PBS twice and collected using cell scrapers, followed by precipitation by centrifugation at 1400×*g* for 3 min. The cells were washed with FACS buffer (1% bovine serum albumin, 0.1% NaN_3 in PBS) once and stained with the primary antibody in FACS buffer on ice for 45 min. After washing with FACS buffer twice, cells were stained with the secondary antibody in FACS buffer on ice for 25 min. Cells were washed with PBS twice and the data were collected with a FACS Melody cell sorter and analyzed by FlowJo software (BD Biosciences). Dilution rates of the antibodies were as follows: anti-CD59 (5H8) (1:100), anti-Prion (4D5) (1:100), anti-FLAG (M2) (1:100), and anti-mouse IgG-PE (1:100 for endogenous prion and 1:500 for endogenous CD59, overexpressed prion, and FLAG).

In silico analysis of hydrophobicity of N-terminal SSs and C-terminal GPI-ASs

The list of GPI-APs was used for the global mapping of hydrophobicity of N-terminal SSs and C-terminal GPI-ASs (21). The hydrophobicity of the N-terminal SSs and C-terminal GPI-ASs from the ω-sites estimated from the UniProtKB database was analyzed using the ExPASy server (https://web.expasy.org/protscale/). The hydropathy score of each amino acid was calculated from a sliding window of nine using the Kyte–Doolittle score (71). The total hydrophobicity score of N-terminal SSs and C-terminal GPI-ASs of each GPI-AP was plotted by two-dimensional plot and is listed in Table S2.

Statistics

Statistical analyses were performed using GraphPad Prism 8 software (GraphPad Software, Inc).

Data availability

All of the data are contained within the article.

Supporting information—This article contains supporting information.

Acknowledgments—We thank Ms Chizuko Yonekawa and Ms Emiko Mori (Gifu University) for technical help. We also thank Edanz (https://jp.edanz.com/ac) for editing a draft of this manuscript.

Author contributions—T. H. conceptualization; T. H., J. Y., and Y. T. investigation; T. H., J. Y., S. T., and Y. T. resources; T. H. writing–original draft; T. H. and Y. K. writing–review & editing; T. H. visualization; T. K., M. F., and Y. K. supervision; Y. K. project administration; T. H. and Y. K. funding acquisition.

Funding and additional information—This work was supported by a Grant-in-Aid for Early-Career Scientists to T. H. (20K15746), an ACT-X grant ((JPMJAX201B) to T. H.) from Japan Science and Technology (JST), a Grant-in-Aid for Scientific Research (B) to Y. K. (20H03207), Leading Initiative for Excellent Young Researchers (LEADER) project (Y. K.) from the Japan Society for the Promotion of Science (JSPS), a CREST grant ((18070267) to Y. K.) from JST, a grant from the Takeda Science Foundation to Y. K., and a grant from the Naito Foundation to Y. K..

Conflict of interest—The authors declare that they have no conflicts of interest with the contents of this article.

Abbreviations—The abbreviations used are: cDNA, complementary DNA; ER, endoplasmic reticulum; FACS, fluorescence-activated cell sorting; GET, guided entry of TA proteins; GPI, glycosylphosphatidylinositol; GPI-AP, GPI-anchored protein; GPI-AS, GPI-attachment signal sequence; HRP, horseradish peroxidase; OST, oligosaccharyltransferase; PGAP, post-GPI attachment to protein; sgRNA, single guide RNA; SRP, signal recognition particle; SS, signal sequence; TA, tail-anchored.

References

1. Wallin, E., and von Heijne, G. (1998) Genome-wide analysis of integral membrane proteins from eubacterial, archaean, and eukaryotic organisms. *Protein Sci.* **7**, 1029–1038
2. Chen, Y., Zhang, Y., Yin, Y., Gao, G., Li, S., Jiang, Y., *et al.* (2005) SPD–a web-based secreted protein database. *Nucleic Acids Res.* **33**, D169–D173
3. Aviram, N., and Schuldiner, M. (2017) Targeting and translocation of proteins to the endoplasmic reticulum at a glance. *J. Cell Sci* **130**, 4079–4085
4. Blobel, G., and Dobberstein, B. (1975) Transfer of proteins across membranes. I. Presence of proteolytically processed and unprocessed nascent immunoglobulin light chains on membrane-bound ribosomes of murine myeloma. *J. Cell Biol* **67**, 835–851

5. Egea, P. F., Stroud, R. M., and Walter, P. (2005) Targeting proteins to membranes: Structure of the signal recognition particle. *Curr. Opin. Struct. Biol.* **15**, 213–220
6. Gemmer, M., and Forster, F. (2020) A clearer picture of the ER translocon complex. *J. Cell Sci* **133**, jcs231340
7. Hann, B. C., and Walter, P. (1991) The signal recognition particle in S. cerevisiae. *Cell* **67**, 131–144
8. Meyer, H. A., Grau, H., Kraft, R., Kostka, S., Prehn, S., Kalies, K. U., *et al.* (2000) Mammalian Sec61 is associated with Sec62 and Sec63. *J. Biol. Chem.* **275**, 14550–14557
9. Kutay, U., Hartmann, E., and Rapoport, T. A. (1993) A class of membrane proteins with a C-terminal anchor. *Trends Cell Biol* **3**, 72–75
10. Hegde, R. S., and Keenan, R. J. (2011) Tail-anchored membrane protein insertion into the endoplasmic reticulum. *Nat. Rev. Mol. Cell Biol* **12**, 787–798
11. Schuldiner, M., Metz, J., Schmid, V., Denic, V., Rakwalska, M., Schmitt, H. D., *et al.* (2008) The GET complex mediates insertion of tail-anchored proteins into the ER membrane. *Cell* **134**, 634–645
12. Stefanovic, S., and Hegde, R. S. (2007) Identification of a targeting factor for posttranslational membrane protein insertion into the ER. *Cell* **128**, 1147–1159
13. Mateja, A., Paduch, M., Chang, H. Y., Szydlowska, A., Kossiakoff, A. A., Hegde, R. S., *et al.* (2015) Protein targeting. Structure of the Get3 targeting factor in complex with its membrane protein cargo. *Science* **347**, 1152–1155
14. Favaloro, V., Vilardi, F., Schlecht, R., Mayer, M. P., and Dobberstein, B. (2010) Asna1/TRC40-mediated membrane insertion of tail-anchored proteins. *J. Cell Sci* **123**, 1522–1530
15. Yamamoto, Y., and Sakisaka, T. (2012) Molecular machinery for insertion of tail-anchored membrane proteins into the endoplasmic reticulum membrane in mammalian cells. *Mol. Cell* **48**, 387–397
16. Vilardi, F., Lorenz, H., and Dobberstein, B. (2011) WRB is the receptor for TRC40/Asna1-mediated insertion of tail-anchored proteins into the ER membrane. *J. Cell Sci* **124**, 1301–1307
17. Wang, F., Chan, C., Weir, N. R., and Denic, V. (2014) The Get1/2 transmembrane complex is an endoplasmic-reticulum membrane protein insertase. *Nature* **512**, 441–444
18. Aviram, N., Ast, T., Costa, E. A., Arakel, E. C., Chuartzman, S. G., Jan, C. H., *et al.* (2016) The SND proteins constitute an alternative targeting route to the endoplasmic reticulum. *Nature* **540**, 134–138
19. Hassdenteufel, S., Sicking, M., Schorr, S., Aviram, N., Fecher-Trost, C., Schuldiner, M., *et al.* (2017) hSnd2 protein represents an alternative targeting factor to the endoplasmic reticulum in human cells. *FEBS Lett.* **591**, 3211–3224
20. Casson, J., McKenna, M., Hassdenteufel, S., Aviram, N., Zimmerman, R., and High, S. (2017) Multiple pathways facilitate the biogenesis of mammalian tail-anchored proteins. *J. Cell Sci* **130**, 3851–3861
21. Yang, J., Hirata, T., Liu, Y. S., Guo, X. Y., Gao, X. D., Kinoshita, T., *et al.* (2021) Human SND2 mediates ER targeting of GPI-anchored proteins with low hydrophobic GPI attachment signals. *FEBS Lett.* **595**, 1542–1558
22. Hassdenteufel, S., Johnson, N., Paton, A. W., Paton, J. C., High, S., and Zimmermann, R. (2018) Chaperone-Mediated Sec61 channel gating during ER import of small precursor proteins overcomes Sec61 inhibitor-reinforced energy barrier. *Cell Rep* **23**, 1373–1386
23. Talbot, B. E., Vandorpe, D. H., Stotter, B. R., Alper, S. L., and Schlondorff, J. S. (2019) Transmembrane insertases and N-glycosylation critically determine synthesis, trafficking, and activity of the nonselective cation channel TRPC6. *J. Biol. Chem.* **294**, 12655–12669
24. Schjoldager, K. T., Narimatsu, Y., Joshi, H. J., and Clausen, H. (2020) Global view of human protein glycosylation pathways and functions. *Nat. Rev. Mol. Cell Biol* **21**, 729–749
25. Narimatsu, Y., Bull, C., Chen, Y. H., Wandall, H. H., Yang, Z., and Clausen, H. (2021) Genetic glycoengineering in mammalian cells. *J. Biol. Chem.* **296**, 100448
26. Kinoshita, T. (2020) Biosynthesis and biology of mammalian GPI-anchored proteins. *Open Biol.* **10**, 190290
27. Liu, Y. S., and Fujita, M. (2020) Mammalian GPI-anchor modifications and the enzymes involved. *Biochem. Soc. Trans.* **48**, 1129–1138
28. Ferguson, M. A. J., Hart, G. W., and Kinoshita, T. (2015) Glycosylphosphatidylinositol anchors. In: Varki, A., Cummings, R. D., Esko, J. D., Stanley, P., Hart, G. W., Aebi, M., *et al.* eds. Essentials of Glycobiology *(3rd*, Cold Spring Harbor, (NY): 137–150
29. Takeda, J., Miyata, T., Kawagoe, K., Iida, Y., Endo, Y., Fujita, T., *et al.* (1993) Deficiency of the GPI anchor caused by a somatic mutation of the PIG-A gene in paroxysmal nocturnal hemoglobinuria. *Cell* **73**, 703–711
30. Almeida, A. M., Murakami, Y., Layton, D. M., Hillmen, P., Sellick, G. S., Maeda, Y., *et al.* (2006) Hypomorphic promoter mutation in PIGM causes inherited glycosylphosphatidylinositol deficiency. *Nat. Med.* **12**, 846–851
31. Bellai-Dussault, K., Nguyen, T. T. M., Baratang, N. V., Jimenez-Cruz, D. A., and Campeau, P. M. (2019) Clinical variability in inherited glycosylphosphatidylinositol deficiency disorders. *Clin. Genet.* **95**, 112–121
32. Hirata, T., Kobayashi, A., Furuse, T., Yamada, I., Tamura, M., Tomita, H., *et al.* (2022) Loss of the N-acetylgalactosamine side chain of the GPI-anchor impairs bone formation and brain functions and accelerates the prion disease pathology. *J. Biol. Chem.* **298**, 101720
33. Evans, E. A., Gilmore, R., and Blobel, G. (1986) Purification of microsomal signal peptidase as a complex. *Proc. Natl. Acad. Sci. U S A.* **83**, 581–585
34. Liaci, A. M., Steigenberger, B., Telles de Souza, P. C., Tamara, S., Grollers-Mulderij, M., Ogrissek, P., *et al.* (2021) Structure of the human signal peptidase complex reveals the determinants for signal peptide cleavage. *Mol. Cell* **81**, 3934–3948.e11
35. Hamburger, D., Egerton, M., and Riezman, H. (1995) Yeast Gaa1p is required for attachment of a completed GPI anchor onto proteins. *J. Cell Biol* **129**, 629–639
36. Yu, J., Nagarajan, S., Knez, J. J., Udenfriend, S., Chen, R., and Medof, M. E. (1997) The affected gene underlying the class K glycosylphosphatidylinositol (GPI) surface protein defect codes for the GPI transamidase. *Proc. Natl. Acad. Sci. U S A.* **94**, 12580–12585
37. Tanaka, S., Maeda, Y., Tashima, Y., and Kinoshita, T. (2004) Inositol deacylation of glycosylphosphatidylinositol-anchored proteins is mediated by mammalian PGAP1 and yeast Bst1p. *J. Biol. Chem.* **279**, 14256–14263
38. Fujita, M., Maeda, Y., Ra, M., Yamaguchi, Y., Taguchi, R., and Kinoshita, T. (2009) GPI glycan remodeling by PGAP5 regulates transport of GPI-anchored proteins from the ER to the Golgi. *Cell* **139**, 352–365
39. Maeda, Y., Tashima, Y., Houjou, T., Fujita, M., Yoko-o, T., Jigami, Y., *et al.* (2007) Fatty acid remodeling of GPI-anchored proteins is required for their raft association. *Mol. Biol. Cell* **18**, 1497–1506
40. Tashima, Y., Taguchi, R., Murata, C., Ashida, H., Kinoshita, T., and Maeda, Y. (2006) PGAP2 is essential for correct processing and stable expression of GPI-anchored proteins. *Mol. Biol. Cell* **17**, 1410–1420
41. Hirata, T., Mishra, S. K., Nakamura, S., Saito, K., Motooka, D., Takada, Y., *et al.* (2018) Identification of a Golgi GPI-N-acetylgalactosamine transferase with tandem transmembrane regions in the catalytic domain. *Nat. Commun.* **9**, 405
42. Wang, Y., Maeda, Y., Liu, Y. S., Takada, Y., Ninomiya, A., Hirata, T., *et al.* (2020) Cross-talks of glycosylphosphatidylinositol biosynthesis with glycosphingolipid biosynthesis and ER-associated degradation. *Nat. Commun.* **11**, 860
43. Ast, T., Cohen, G., and Schuldiner, M. (2013) A network of cytosolic factors targets SRP-independent proteins to the endoplasmic reticulum. *Cell* **152**, 1134–1145
44. Lang, S., Benedix, J., Fedeles, S. V., Schorr, S., Schirra, C., Schauble, N., *et al.* (2012) Different effects of Sec61alpha, Sec62 and Sec63 depletion on transport of polypeptides into the endoplasmic reticulum of mammalian cells. *J. Cell Sci* **125**, 1958–1969
45. Davis, E. M., Kim, J., Menasche, B. L., Sheppard, J., Liu, X., Tan, A. C., *et al.* (2015) Comparative haploid genetic screens reveal divergent pathways in the biogenesis and trafficking of glycophosphatidylinositol-anchored proteins. *Cell Rep* **11**, 1727–1736
46. Ng, D. T., Brown, J. D., and Walter, P. (1996) Signal sequences specify the targeting route to the endoplasmic reticulum membrane. *J. Cell Biol* **134**, 269–278

47. Kurzchalia, T. V., Wiedmann, M., Girshovich, A. S., Bochkareva, E. S., Bielka, H., and Rapoport, T. A. (1986) The signal sequence of nascent preprolactin interacts with the 54K polypeptide of the signal recognition particle. *Nature* **320**, 634–636
48. Galian, C., Bjorkholm, P., Bulleid, N., and von Heijne, G. (2012) Efficient glycosylphosphatidylinositol (GPI) modification of membrane proteins requires a C-terminal anchoring signal of marginal hydrophobicity. *J. Biol. Chem.* **287**, 16399–16409
49. Walmsley, A. R., Watt, N. T., Taylor, D. R., Perera, W. S., and Hooper, N. M. (2009) alpha-cleavage of the prion protein occurs in a late compartment of the secretory pathway and is independent of lipid rafts. *Mol. Cell Neurosci* **40**, 242–248
50. Cherepanova, N., Shrimal, S., and Gilmore, R. (2016) N-linked glycosylation and homeostasis of the endoplasmic reticulum. *Curr. Opin. Cell Biol* **41**, 57–65
51. Shrimal, S., Cherepanova, N. A., and Gilmore, R. (2015) Cotranslational and posttranslocational N-glycosylation of proteins in the endoplasmic reticulum. *Semin. Cell Dev Biol* **41**, 71–78
52. Liu, Y. S., Guo, X. Y., Hirata, T., Rong, Y., Motooka, D., Kitajima, T., *et al.* (2018) N-Glycan-dependent protein folding and endoplasmic reticulum retention regulate GPI-anchor processing. *J. Cell Biol* **217**, 585–599
53. Menon, A. K. (1994) Structural analysis of glycosylphosphatidylinositol anchors. *Methods Enzymol.* **230**, 418–442
54. Heinz, D. W., Ryan, M., Bullock, T. L., and Griffith, O. H. (1995) Crystal structure of the phosphatidylinositol-specific phospholipase C from Bacillus cereus in complex with myo-inositol. *EMBO J.* **14**, 3855–3863
55. Schorr, S., Nguyen, D., Hassdenteufel, S., Nagaraj, N., Cavalie, A., Greiner, M., *et al.* (2020) Identification of signal peptide features for substrate specificity in human Sec62/Sec63-dependent ER protein import. *FEBS J.* **287**, 4612–4640
56. Brodsky, J. L., Goeckeler, J., and Schekman, R. (1995) BiP and Sec63p are required for both co- and posttranslational protein translocation into the yeast endoplasmic reticulum. *Proc. Natl. Acad. Sci. U S A.* **92**, 9643–9646
57. Matlack, K. E., Plath, K., Misselwitz, B., and Rapoport, T. A. (1997) Protein transport by purified yeast Sec complex and Kar2p without membranes. *Science* **277**, 938–941
58. Tyedmers, J., Lerner, M., Wiedmann, M., Volkmer, J., and Zimmermann, R. (2003) Polypeptide-binding proteins mediate completion of cotranslational protein translocation into the mammalian endoplasmic reticulum. *EMBO Rep.* **4**, 505–510
59. Sun, S., and Mariappan, M. (2020) C-terminal tail length guides insertion and assembly of membrane proteins. *J. Biol. Chem.* **295**, 15498–15510
60. O'Keefe, S., Zong, G., Duah, K. B., Andrews, L. E., Shi, W. Q., and High, S. (2021) An alternative pathway for membrane protein biogenesis at the endoplasmic reticulum. *Commun. Biol.* **4**, 828
61. Gorlich, D., and Rapoport, T. A. (1993) Protein translocation into proteoliposomes reconstituted from purified components of the endoplasmic reticulum membrane. *Cell* **75**, 615–630
62. Paladino, S., Lebreton, S., Tivodar, S., Campana, V., Tempre, R., and Zurzolo, C. (2008) Different GPI-attachment signals affect the oligomerisation of GPI-anchored proteins and their apical sorting. *J. Cell Sci* **121**, 4001–4007
63. Puig, B., Altmeppen, H. C., Thurm, D., Geissen, M., Conrad, C., Braulke, T., *et al.* (2011) N-glycans and glycosylphosphatidylinositol-anchor act on polarized sorting of mouse PrP(C) in Madin-Darby canine kidney cells. *PLoS One* **6**, e24624
64. Puig, B., Altmeppen, H. C., Linsenmeier, L., Chakroun, K., Wegwitz, F., Piontek, U. K., *et al.* (2019) GPI-anchor signal sequence influences PrPC sorting, shedding and signalling, and impacts on different pathomechanistic aspects of prion disease in mice. *Plos Pathog.* **15**, e1007520
65. Miyagawa-Yamaguchi, A., Kotani, N., and Honke, K. (2014) Expressed glycosylphosphatidylinositol-anchored horseradish peroxidase identifies co-clustering molecules in individual lipid raft domains. *PLoS One* **9**, e93054
66. Paladino, S., Sarnataro, D., Pillich, R., Tivodar, S., Nitsch, L., and Zurzolo, C. (2004) Protein oligomerization modulates raft partitioning and apical sorting of GPI-anchored proteins. *J. Cell Biol* **167**, 699–709
67. Lee, G. H., Fujita, M., Nakanishi, H., Miyata, H., Ikawa, M., Maeda, Y., *et al.* (2020) PGAP6, a GPI-specific phospholipase A2, has narrow substrate specificity against GPI-anchored proteins. *J. Biol. Chem.* **295**, 14501–14509
68. Hirata, T., Fujita, M., Nakamura, S., Gotoh, K., Motooka, D., Murakami, Y., *et al.* (2015) Post-Golgi anterograde transport requires GARP-dependent endosome-to-TGN retrograde transport. *Mol. Biol. Cell* **26**, 3071–3084
69. Hirata, T., Nagae, M., Osuka, R. F., Mishra, S. K., Yamada, M., and Kizuka, Y. (2020) Recognition of glycan and protein substrates by N-acetylglucosaminyltransferase-V. *Biochim. Biophys. Acta Gen. Subj* **1864**, 129726
70. Kitajima, T., Xue, W., Liu, Y. S., Wang, C. D., Liu, S. S., Fujita, M., *et al.* (2018) Construction of green fluorescence protein mutant to monitor STT3B-dependent N-glycosylation. *FEBS J.* **285**, 915–928
71. Kyte, J., and Doolittle, R. F. (1982) A simple method for displaying the hydropathic character of a protein. *J. Mol. Biol.* **157**, 105–132